Geomechanics and Engineering, *Vol. 15, No. 6 (2018) 1183-1191*
DOI: https://doi.org/10.12989/gae.2018.15.6.1183

Reliability analysis of three-dimensional rock slope

X.L. Yang* and Z.A. Liu[a]

School of Civil Engineering, Central South University, Hunan 410075, China

(Received October 21, 2017, Revised March 14, 2018, Accepted April 13, 2018)

Abstract. Reliability analysis is generally regarded as the most appropriate method when uncertainties are taken into account in slope designs. With the help of limit analysis, probability evaluation for three-dimensional rock slope stability was conducted based upon the Mote Carlo method. The nonlinear Hoek-Brown failure criterion was employed to reflect the practical strength characteristics of rock mass. A form of stability factor is used to perform reliability analysis for rock slopes. Results show that the variation of strength uncertainties has significant influence on probability of failure for rock slopes, as well as strength constants. It is found that the relationship between probability of failure and mean safety factor is independent of the magnitudes of input parameters but relative to the variability of variables. Due to the phenomenon, curves displaying this relationship can provide guidance for designers to obtain factor of safety according to required failure probability.

Keywords: rock slope; reliability analysis; Hoek-Brown criterion; limit analysis

1. Introduction

The linear Mohr-Coulomb (MC) criterion is often used in practical rock engineering owing to its simplicity and practicability. However, experiments have demonstrated that the linear criterion is not suitable for rock materials whose strength envelopes present nonlinearity (Cai *et al*. 2007, Yang and Li 2018a). In order to provide input data for the design of underground excavations in hard rock mass, Hoek and Brown (1980) proposed the Hoek-Brown failure criterion. This nonlinear criterion was later modified by Hoek *et al*. (2002) to describe the strength characteristics of rock more accurately.

Two-dimensional (2D) plane strain analysis has been adopted to estimate stability of slopes over several decades as the 2D analysis is generally considered to be conservative. However, the conservative factors of safety in the 2D analysis will be obtained only if the most pessimistic partition in the three-dimensional (3D) question is selected, and 3D mechanism is more critical and realistic under some conditions (Griffiths and Marquez 2007). The limit equilibrium method and the finite element method have been employed to estimate stability of 3D slopes (Hungr 1987). However, the limit equilibrium method entails some assumptions to meet the relevant requirements, and the finite element method demands specific slopes with accurate geotechnical parameters. The limit analysis approach overcomes these difficulties, therefore, this theory is more suitable for 3D analysis of slopes. Michalowski (1989) proposed a 3D multi-block mechanism of slope failure within limit analysis. Furthermore, a 3D horn failure mechanism was put forward for 3D slope.

Reliability methods used for estimating the safety of earth slopes was earliest used in the 1970s. The randomness of strength parameters, geometries properties, and material properties can be taken into account in reliability methods, and accordingly designs based on these methods will be more rational and practical. Numerous researches have been conducted with respect to the failure of soil or rock slopes by virtue of reliability analysis (Al-Homoud and Tanash 2004, Cassidy *et al*. 2008, Li and Lumb 1987, Low 2007, Shinoda 2007). However, these reliability analyses of slopes are generally in conjunction with limit equilibrium analysis, rather than limit analysis. Li *et al*. (2012) combined limit analysis with reliability method to study stability of 2D rock slopes. In the present analysis, 3D rock slopes under the effect of seismic load will be investigated. The nonlinear HB failure criterion is employed to depict the strength characteristics of rock mass, and the combined method of the limit analysis method and the Monte Carlo method is adopted to evaluate corresponding rock slope stability.

2. Stability analysis of 3D rock slopes

2.1 HB failure criterion and generalized tangential technique

MC soil parameters (c and φ) are required by most computer programs to analyze slope stability. However, the non-linear nature of the rock mass failure envelope is more pronounced at the low confining stresses which is operational in slope stability problems (Xu *et al*. 2018, Xu and Yang 2018a, Xu and Yang 2018b, Yang and Li 2018b). The HB failure criterion is one of the few non-linear criteria utilized by practicing engineers to estimate rock mass strength. Hoek and Brown (1980) first proposed the HB failure criterion in 1980, and the latest version of this

*Corresponding author, Professor
E-mail: yangky@aliyun.com
[a]M.S. Student

ISSN: 2005-307X (Print), 2092-6219 (Online)

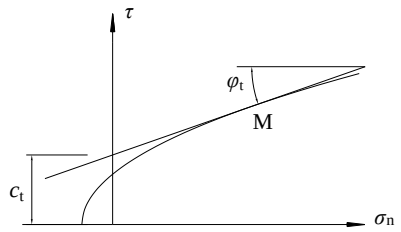

Fig. 1 Tangential line to the modified Hoek-Brown failure criterion

criterion is presented as (Hoek *et al*. 2002)

$$\sigma_1 = \sigma_3 + \sigma_c \left(m\sigma_3 / \sigma_c + s \right)^n \tag{1}$$

$$m = m_i \exp\left(\frac{GSI - 100}{28 - 14D} \right) \tag{2}$$

$$s = \exp\left(\frac{GSI - 100}{9 - 3D} \right) \tag{3}$$

$$n = 0.5 + \left(e^{-GSI/15} - e^{-20/3} \right) / 6 \tag{4}$$

where σ_c is the intact uniaxial compressive strength, m_i is the material constant and D represents the disturbance degree of rock mass. As illustrated in the above equations, the magnitudes of m, s and n are determined by geological strength index (*GSI*) and D.

The tangential line to curve at location of tangency point M, is shown in Fig. 1. The tangential line is (Zhang and Chen 1987, Huang *et al*. 2018)

$$\tau = c_t + \sigma_n \tan\varphi_t \tag{5}$$

where φ_t and c_t are the tangential friction angle and the intercept of the straight line with τ-axis respectively. c_t is expressed as (Yang and Zhang 2018a, Yang and Zhang 2018b)

$$\frac{c_t}{\sigma_c} = \left[\frac{\cos\varphi_t}{2} - \frac{\tan\varphi_t}{m}\left(1 + \frac{\sin\varphi_t}{n} \right) \right] \times \left[\frac{mn(1-\sin\varphi_t)}{2\sin\varphi_t} \right]^{\frac{1}{1-n}} + \frac{s}{m}\tan\varphi_t \tag{6}$$

It can be seen that the tangential line is above the nonlinear failure criterion, therefore the linear failure criterion represented by the tangential line will give an upper bound of the actual load for the material, whose failure envelope is nonlinear.

2.2 Construction of 3D failure mechanism

Limit analysis is widely used in civil engineering (Li and Yang 2018a, Li and Yang 2018b, Yang and Wang 2018). Xu and Yang (2018b) studied a homogenous slope with angles α and β, as show in Fig. 2. The slope is subjected to earthquake forces, which is described by a horizontal seismic coefficient k_h. Michalowski and Drescher (2009) proposed the 3D failure mechanism whose shape is a curvilinear cone with apex angle, as shown in Fig. 2. This failure mechanism has one symmetry plane passing the toe point C, and partially intersects the rock slope. The trace of the mechanism on the symmetry plane is described by two

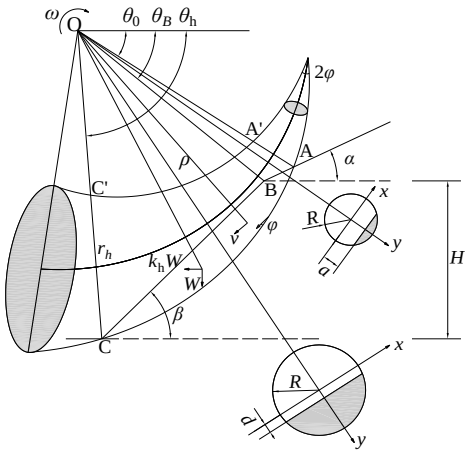

Fig. 2 Three-dimensional rotational mechanism of slope with inclined angle

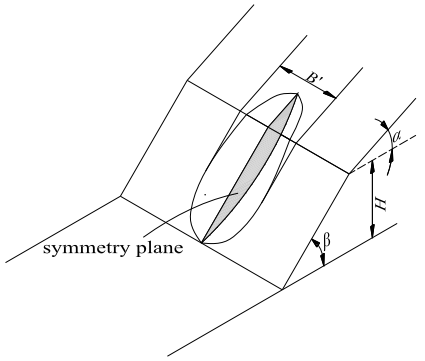

(a) 3D rotational mechanism with inclined angle

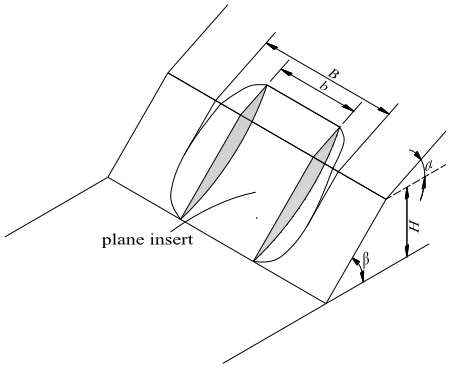

(b) 3D mechanism with plane insert

Fig. 3 Schematic diagram of three-dimensional mechanism with inclined angle

log-spirals, AC

$$r = r_0 e^{(\theta - \theta_0)\tan\phi} \tag{7}$$

and A'C'

$$r' = r_0' e^{-(\theta - \theta_0)\tan\varphi_t} \tag{8}$$

where OA= r_0, O'A'= r_0'. Given angles θ_0 and θ_h, and the ratio r_0' / r_0, the location of the horn surface in the space can be uniquely determined.

Furthermore, the critical height is not only related with slope angles and strength parameters, but also with the

width of sliding block (Michalowski and Drescher 2009, Yang and Li 2018b). In view of this case, a plane insert is appended to the 3D failure patterns (Fig. 3(a)) to make the result consistent with practice. As illustrated in Fig. 3(b), the 3D surface is divided into two halves. The new parameter, *b*, is named as the width of the insert block, and *B* is the sum of rotational mechanism subjecting to a limitation imposed on the maximum of slope width.

2.3 A new non-dimensional stability factor

The stability factor is defined as

$$N_n = \frac{\gamma H_c}{\sqrt{s}\sigma_c} \tag{9}$$

where γ is the unit weight of the rock mass, and H_c is the minimum upper solution of the critical height of rock slope under earthquake forces. The critical height is expressed as

$$H = \frac{c_t \cot\varphi_t \sin\beta}{\gamma \sin(\beta-\alpha)}\left[\sin(\theta_h+\alpha)e^{(\theta_h-\theta_0)\tan\varphi_t} - \sin(\theta_0+\alpha)\right] \times \frac{g_5(\theta_0,\theta_h,r_0^{'}/r_0)+g_6(\theta_0,\theta_h,b/H)}{g_1(\theta_0,\theta_h,r_0^{'}/r_0)+g_2(\theta_0,\theta_h,b/H)+k_h g_3(\theta_0,\theta_h,r_0^{'}/r_0)+k_h g_4(\theta_0,\theta_h,b/H)} \tag{10}$$

where g_1, g_2, g_3, g_4, g_5, and g_6 are given in Xu and Yang (2018b), with the following constraint conditions, as shown in Eq. (11).

$$\begin{cases} 0<\theta_0<\pi \\ \theta_0<\theta_h<\pi \\ 0<r_0^{'}/r_0<1 \\ 1<\varphi_t<\pi/2 \\ 0<\left(b+B_{\max}^{'}\right)/H<B/H \end{cases} \tag{11}$$

where $B_{\max}^{'}$ is the maximum width of rotation mechanism and *B* is the finite width of slope. Li *et al*. (2012) proposed the safety factor defined as

$$F = \frac{\sigma_c}{\gamma H N} \tag{12}$$

where *N* is the dimensionless stability number and it is different from the stability factor N_n mentioned above. The safety factor is adopted to analyze the stability of rock slopes in limit analysis method which is the same as the conventional factor of safety used in limit equilibrium, as shown in Eq. (13). But *F* and F_s generally are not equal (i.e., $F \neq F_s$) due to their different definitions.

$$F_s = \frac{\sum(\text{resisting actions})}{\sum(\text{driving actions})} \tag{13}$$

In terms of a slope with a height of *H*, the stability factor can be expressed as

$$N_n^{'} = \frac{\gamma H}{\sqrt{s}\sigma_c} \tag{15}$$

Corresponding stability factor with H_c of the slope is shown in Eq. (9). Then, the safety factor can be derived from Eq. (15), and it is shown in Eq. (16). Finally, the new non-dimensional stability factor can be presented as Eq. (17). A purpose of this paper is to calibrate the new safety factor expressed in Eq. (16) for different probability of failures.

$$F = N_n^{'} / N_n \tag{16}$$

$$F = \frac{N_n \sqrt{s}\sigma_c}{\gamma H} \tag{17}$$

$$N_n = \frac{\gamma H F}{\sqrt{s}\sigma_c} \tag{18}$$

3. Reliability estimation of rock slope

3.1 Determination of random variables

In the limit analyses, for given slope geometry (α, β, *B/H*), rock mass (σ_c, *GSI*, m_i, *D*, and γ), and seismic coefficient (k_h), the optimized solutions of the critical height can be carried out with respect to the constraint conditions. Therefore, the stability factor can be derived from Eq. (9). However, as regards probabilistic analyses, the slope height (*H*) is required as an extra input, as well as parameters above.

The first priority is to determine all uncertainties in rock slopes for reliability analysis. Hoek (1998) proposed that σ_c, m_i, and *GSI* were distributed normally with their coefficients of variation (*COVs*) being 0.25, 0.125, and 0.1 respectively. Li *et al*. (2012) adopted the standard deviation (*Stdev*) of 2.5 for *GSI* instead of *COV* equaling to 0.1, as *Stdev* changes slightly with different *GSI* estimates. Therefore, these three parameters are regarded as uncertainties for reliability assessment, and above *COVs* or *Stdev* of random variables are adopted in the study. One case in critical situation is utilized for the following probability analysis, as shown in Table 1.

3.2 Application of Monte Carlo method

Monte Carlo method can estimate the failure probability (P_f) through the proportion of failure cases. Four steps need to be executed to realize the reliability method: (1) All

Table 1 Input parameters

Item	Mean	*COV* or *Stdev*
σ_c	1 MPa	0.25(*COV*)
m_i	15	0.125(*COV*)
GSI	50	2.5(*Stdev*)
D	0	-
H	52 m	-
α	15°	-
β	60°	-
B/H	5	-
γ	20 kN/m^3	-
k_h	0.05	-

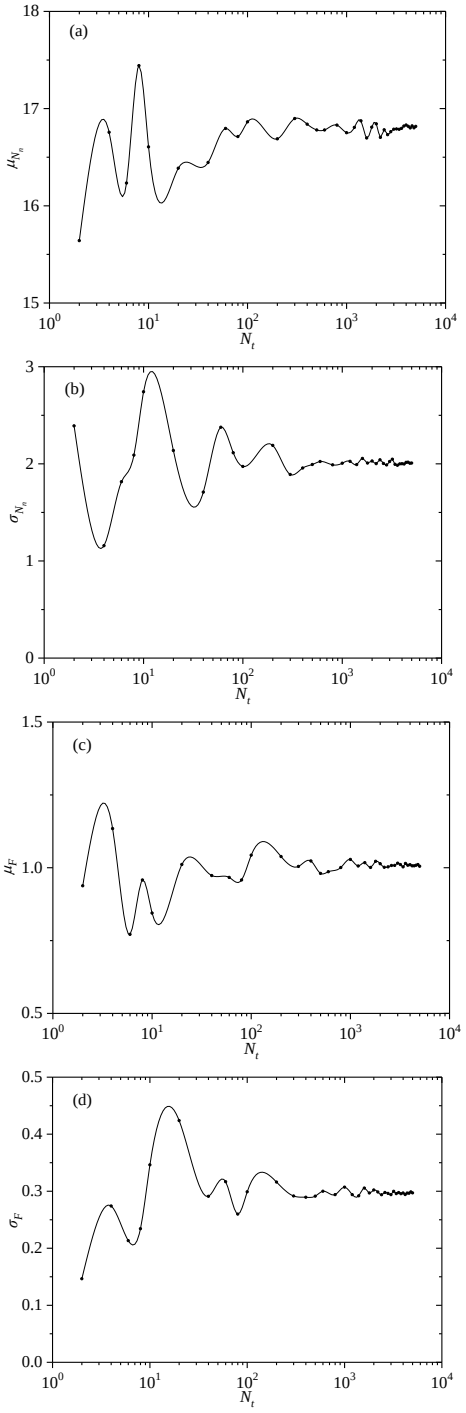

Fig. 4 Influences of the number of Monte Carlo simulations on results (a) μ_{N_n}–N_t; (b) σ_{N_n}–N_t; (c) μ_F–N_t; (d) σ_F–N_t

random variables (σ_c, m_i, *GSI*) are sampled with N_t times to generate N_t samples, where N_t is the total amount of samples, and each sample comprise whole uncertainties (σ_c, m_i, *GSI*); (2) Every sample as well as other parameters (D, α, β, B/H, γ, and k_h) is substituted one by one into optimization program, then N_t stability factors are obtained; (3) N_t safety factors can be derived from Eq. (16), and the number of all failure cases (F<1), n_f, is recorded; (4) The failure probability can be calculated with the equation finally.

Table 2 Comparison between the previous stability factor and the present stability factor

Case	*GSI*	N_n		Difference (%)
		Previous	Present	
1	10	11.73	11.99	2.22
2	20	18.51	19.16	3.53
3	30	19.95	20.76	4.05
4	40	18.54	19.27	3.91
5	50	16.25	16.96	4.34
6	60	13.93	14.36	3.10
7	70	12.03	12.19	1.34
8	80	10.24	10.30	0.63

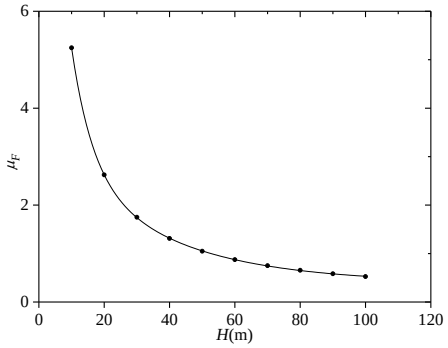

Fig. 5 Relation between mean safety factors and slope height for case 1

$$P_f = \frac{n_f}{N_t} \tag{19}$$

The total amount of samples, N_t, can be obtained by the correlation between the mean and standard deviation of the stability factor (μ_{N_n}, σ_{N_n}) or the safety factor (μ_F, σ_F) and the number of simulations. Fig. 4 shows μ_{N_n}, σ_{N_n}, μ_F, and σ_F as a function of the number of samples for the case presented in Table 1. It indicates that results become stable as the amount of samples reaches N_t=5000. Therefore, the following research is based on 5000 Monte Carlo simulations, which is considered enough to give reasonably stable and reproducible reliability results.

In order to verify the rationality of the reliability method and the new safety factor, some cases are recalculated by reliability analysis, as shown in Table 2. All cases have same parameter values presented in Table 1 except *GSI*. By changing the slope height (H), the relationship between the mean factor of safety and the slope height is presented in Fig. 5, for case 1 in Table 2. The exponential function relationship between μ_F and H is obtained with the help of nonlinear curve fitting tool of *Origin* software. Then the optimized critical height of rock slope (H_c) can be obtained by the exponential function with mean safety factor equaling to 1 (i.e., μ_F=1). The present stability factors can be finally derived by substituting H_c into Eq. (9). From Table 2, it is found that the maximum difference is less than 4.5%. The agreement shows that the reliability method is an effective approach, and uncertainties of rock slope cause the difference between the previous stability factor and the present stability factor.

Table 3 Distribution types of σ_c, m_i, and *GSI* under different combinations (normal distribution and lognormal distribution are presented by N and L respectively)

Combination	σ_c	m_i	*GSI*
C1	N	N	N
C2	N	N	L
C3	N	L	N
C4	L	N	N
C5	N	L	L
C6	L	N	L
C7	L	L	N
C8	L	L	L

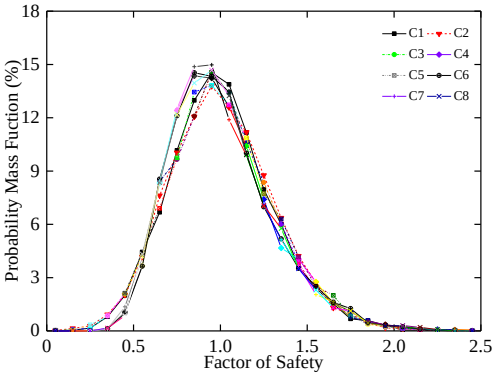

Fig. 6 Distributions of safety factors under different combinations of distribution types of σ_c, m_i, and *GSI*

4. Results and discussions

4.1 Influence of distribution types

As stated previously, three random variables (σ_c, m_i, *GSI*) are adopted for reliability analysis of 3D rock slopes, and input parameters presented in Table 1 are used in this section. The distribution types of random variables comprise of normal distribution and lognormal distribution for strength parameters. Although Hoek (1998) introduced normal distributions of σ_c, m_i, and *GSI*, using a lognormal distribution can ensure positive values of strength parameters to guarantee physical meaning. This part focuses on influence of these two distributions on results of reliability analysis.

In Table 3, there are eight combinations of distribution types of σ_c, m_i, and *GSI*. For convenience, 8 combinations are represented by C1 to C8, respectively. Fig. 6 and Table 4 display the influence of distribution types of σ_c, m_i and *GSI* on distributions of safety factors and the probability of failure respectively. The shapes of the safety factor distributions are similar, and all curves are left-leaning. In Table 4, the probability of failure changes as combination of distribution types of σ_c, m_i, and *GSI* alters. When C1 and C4, C2 and C6, C3 and C7, C5 and C8 are compared with each other, it can be seen that the lognormal distribution of σ_c causes more conservative results. Similarly, lognormal distributions of m_i, and *GSI* make higher and less probability of failure respectively, but both parameters have less influence on results. Overall, there is little effect on the

Table 4 Probability of failure under different combinations of distribution types of σ_c, m_i and *GSI*

C1	C2	C3	C4	C5	C6	C7	C8
51.78%	51.06%	52.14%	54.14%	51.74%	54.26%	56.38%	54.44%

Table 5 Probability of failure in different situations

Situations	*COVs*=0.1	*COVs*=0.2	*COVs*=0.3
Unsafe	91.02%	79.56%	73.44%
Critical	50.00%	53.06%	52.64%
Safe	3.74%	17.4%	27.26%

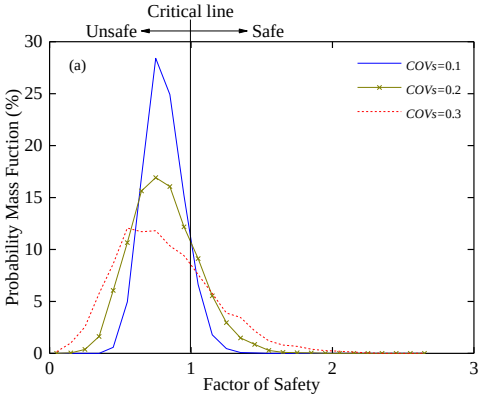

(a) Distribution of the safety factor in unsafe situation (H=65 m)

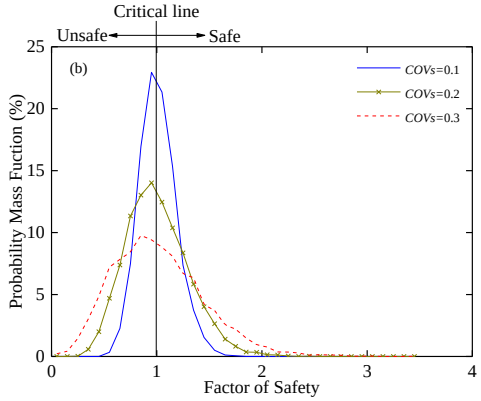

(b) Distribution of the safety factor in critical situation (H=52 m)

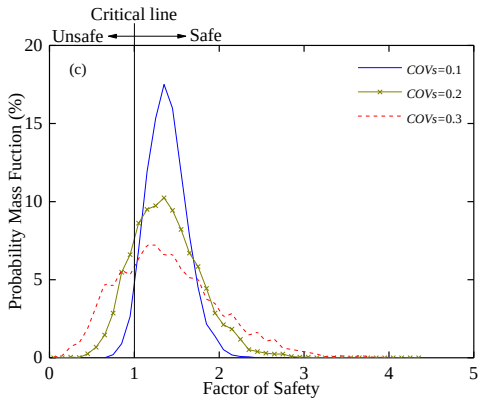

(c) Distribution of the safety factor in safe situation (H=38 m)

Fig. 7 The influence of the *COVs* values in different situations

final results for both distribution types.

4.2 Investigation of coefficient of variation

As pointed by some scholars (Luo and Li 2016), P_f increases, i.e., reliability decreases, when the *COV*s values of variables are augmented. However, the conclusion is inferred as slopes in safe situation (i.e., F>1). In this part, three situations, namely, safe situation (H=38 m), critical situation (H=52 m), and unsafe situation (H=65 m), are considered. Results are displayed in Table 5 and Fig. 7. In Table 5, P_f has different response to variation of the *COV*s values of variables (σ_c, m_i) in different situations. When a slope is safe, P_f increases as the *COV*s values increase; on the contrary, there is a negative correlation between P_f and the *COV*s values under the unsafe situation. However, an alteration of *COV*s values has little influence on P_f as a slope is in critical situation.

There is an explanation of this phenomenon, which can be obtained by Fig. 7. In Fig. 7, an apparent trend is that the distribution of the safety factor becomes wider as the *COV*s values increase and the mean of safety factor is nearly constant. This trend causes the augmentation of the proportion of left and right marginal areas between curve and abscissa. This change finally results in an increase in safe area (for unsafe situation), or unsafe area (for safe situation), so P_f of unsafe slopes decreases but P_f of safe slopes increases. However, P_f of critical slopes fluctuates a little around 50% because the distribution of the safety factor is nearly symmetrical with respect to the critical line (i.e., F=1). So, the *COV*s values have different influences on reliability analysis when a slope is in different situations, as shown in Table 5.

Finally, it is pointed out that the coefficient of variation of variables has a great influence on slopes design progress because of the guarantee of safety (F>1), according to the discussion above.

4.3 The effect of two constants (D, k_h) on reliability assessment

Although studying variables is predominant in probability analysis, it is still worthy of investigating the influence of disturbance factor and seismic coefficient on the P_f evaluations.

There are two situations considered. The first is critical situation, and the second is safe situation. Slope heights of two situations are 52 m and 30 m respectively. There are six cases under critical situation or safe situation as shown in Table 6, and parameters of all cases are same as the case in Table 1, except for *COV* values of σ_c and m_i (*COV*=0.1 for both variables).

Results are presented in Table 7 and Table 8. Whenever slopes are critical or safe, disturbance factor has a great influence on reliability results. However, compared to Table 7, P_f does not increase remarkably with augmentation of k_h for slopes under safe critical situation. As presented in Fig. 8, the distribution of safety factor is narrower and the mean is closer to 1 when both D and k_h increase. In Fig. 8(b), the proportion of unsafe cases is still low, though the influence of k_h is apparent. Briefly, D and k_h have a great influence on distribution of safety factor whenever slopes are in critical or safe situations. Finally, this influence results in a visible change of P_f in reliability analysis.

Table 6 Cases under critical situation (H=52 m) or safe situation (H=30 m)

Case	D	k_h	H
a	0	0.05	30 m or 52 m
b	0.2	0.05	30 m or 52 m
c	0.4	0.05	30 m or 52 m
d	0	0	30 m or 52 m
e	0	0.05	30 m or 52 m
f	0	0.1	30 m or 52 m

Table 7 Probability of failure for cases under critical situation (H=52 m)

Case (a)	Case (b)	Case (c)	Case (d)	Case (e)	Case (f)
51.26%	88.36%	99.56%	15.06%	50.72%	91.52%

Table 8 Probability of failure for cases under safe situation (H=30 m)

Case (a)	Case (b)	Case (c)	Case (d)	Case (e)	Case (f)
0.14%	2.76%	30.62%	0.06%	0.2%	4.2%

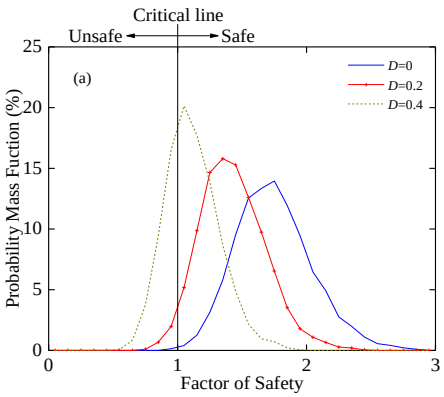

(a) The influence of D

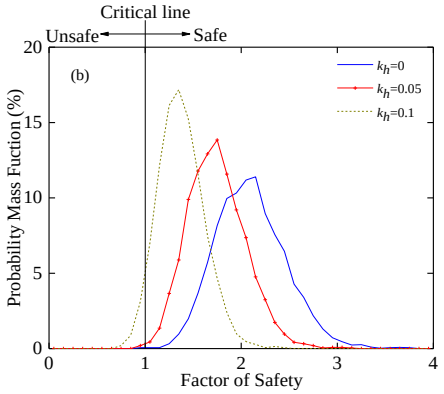

(b) The influence of k_h

Fig. 8 The distribution of safety factor for safe cases (H=30 m)

4.4 Relationship between probability of failure and mean safety factor

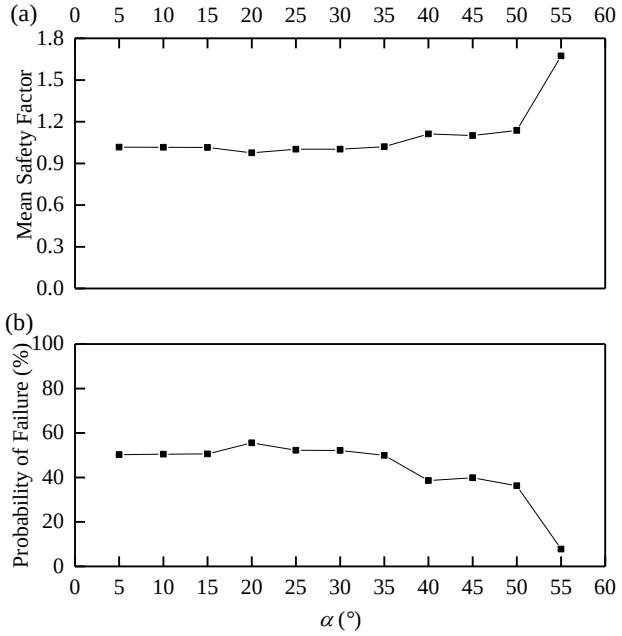

Fig. 9 For case in Table1 (a) Relation between mean safety factor and α, and (b) Relation between probability of failure and α

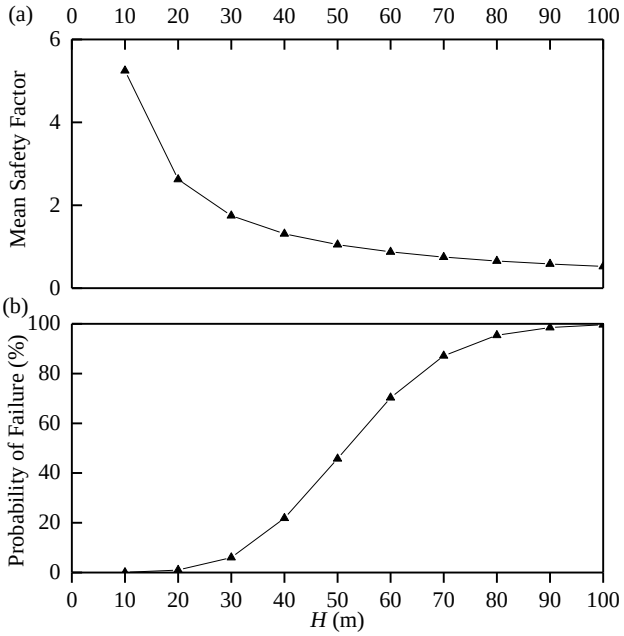

Fig. 11 For case in Table1 (a) Relation between mean safety factor and H, and (b) Relation between probability of failure and H

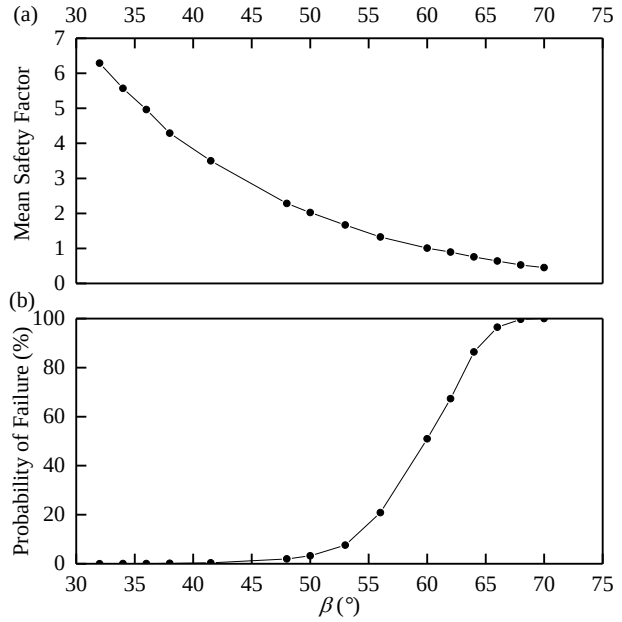

Fig. 10 For case in Table1 (a) Relation between mean safety factor and β, and (b) Relation between probability of failure and β

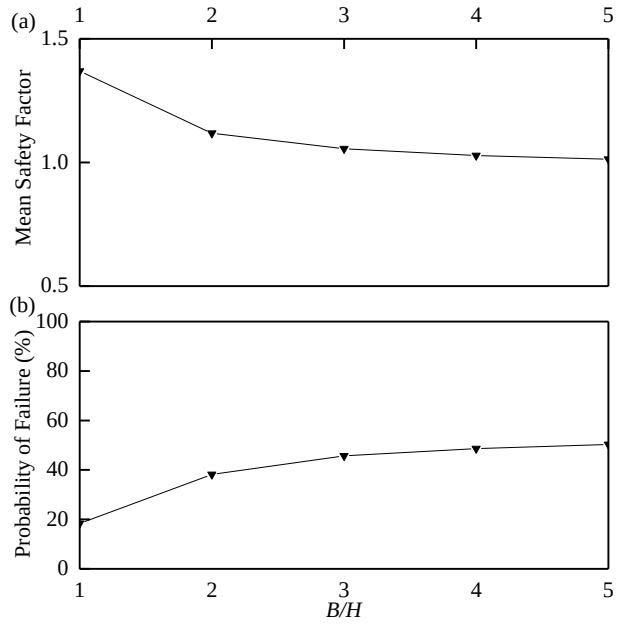

Fig. 12 For case in Table1 (a) Relation between mean safety factor and B/H, and (b) Relation between probability of failure and B/H

Safety factor is usually used to give guidance for design progress of slopes. However, reliability analysis focuses on probability of failure, which reflects safety degree of slopes. A slope is safe when safety factor is more than 1, but it is still unknown whether the slope is safe enough or not. So, it is necessary to study the relationship between probability of failure (P_f) and mean safety factor (μ_F).

The case, whose parameters are given in Table 1, is adopted in next research. Results presented in Fig. 9 to Fig. 12 display the relationship between P_f, μ_F and geometric parameters (α, β, H and B/H). As shown in Fig. 9, α has a little influence on reliability results when α is lower than 50°. However, it is presented that in Fig. 10 to Fig. 12 that the mean safety factor increases with the reduction in other geometric parameters. As expected, probability of failure and these three geometric parameters are negatively correlated. In addition to the trend, β and H have a great effect on reliability results compared with B/H. From the results in Fig. 9 to Fig. 12, the relation between probability of failure and the factor of safety can be derived. The

Table 9 Input parameters for relationship between probability of failure and mean safety factor

Case	*GSI* (*Stdev*=2.5)	σ_c(MPa) (*COV*=0.25)	m_i (*COV*=0.125)	*D*	γ (kN/m^3)	k_h
a1	40	1	15	0	20	0.05
a2	60	1	15	0	20	0.05
b1	50	3	15	0	20	0.05
b2	50	5	15	0	20	0.05
c1	50	1	12	0	20	0.05
c2	50	1	18	0	20	0.05
d1	50	1	15	0.1	20	0.05
d2	50	1	15	0.2	20	0.05
e1	50	1	15	0	15	0.05
e2	50	1	15	0	25	0.05
f1	50	1	15	0	20	0
f2	50	1	15	0	20	0.1

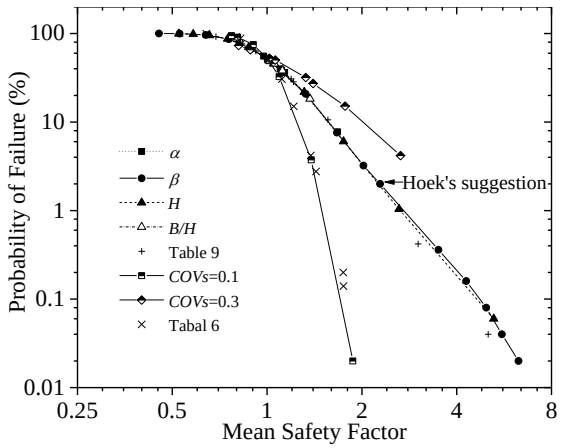

Fig. 13 The relation between probability of failure and mean factors of safety

relationship is displayed in Fig. 13 for all geometric parameters, which are similar. This phenomenon is also valid for slopes whose failure mechanism bases on plane in Li *et al*. (2012).

In order to discuss whether values of rock mass properties (*GSI*, σ_c, m_i, *D*, and γ) and seismic coefficient (k_h) have an influence on the relationship between P_f and μ_F, some cases in Table 9 are adopted. Every case has only one different parameter compared with case in Table 1. Each case is represented by one point in Fig. 13. It is obvious that all cases agree with the relationship between P_f and μ_F derived from geometric parameters. Therefore, the relationship between P_f and μ_F have little correlation with magnitudes of geometries, rock mass properties, and seismic coefficient. However, if *COVs* values of variables change, curves indicating this relation will make changes. As shown in Fig. 13, when *COVs* values are higher, more higher safety factor is required to maintain the same P_f, which means reinforcement or ground improvement should be considered. In addition, cases in Table 6 (*COVs*=0.1) also conforms to the curve for *COVs* of variables (σ_c, m_i) equating to 0.1. As the relationship between P_f and μ_F is independent of the magnitudes of input parameters but relative to variability of uncertainties, the relation can be determined once *COVs* of variables are obtained with the help of sufficient experimental and field measured data. And then, more actual curves will be presented in Fig. 13.

According to the relationship between P_f and μ_F based on the *COVs* of variables suggested by Hoek (1998) in Fig. 13, reliability analysis can provide guidance for slope designs when no further sample and data information is available. Given a failure probability (P_f), the factor of safety can be obtained from Fig. 13. For example, if *COVs* of variables are same as the case in Table 1 and the failure of probability was set to be less than 10^{-3}, then a safety factor of *F*=4.8 could be appropriate. However, if *COVs* of variables is equal to 0.1, *F*=1.7 is adopted for $P_f \leq 10^{-3}$.

5. Conclusions

The present study focuses on the application of reliability analysis for 3D rock slopes based on the HB failure criterion, within the framework of limit analysis. The horn failure mechanism proposed by Michalowski and Drescher (2009) was adopted for the Reliability estimation of rock slopes. For the convenience of risk analysis, the new factor of safety was proposed based upon the stability factor. The purpose of the present work is to calibrate the new safety factor for different probability of failures, which is shown in Fig. 13.

The determination of all variables in rock slopes predominates in reliability analysis. Three parameters (σ_c, m_i, and *GSI*) are regarded as uncertainties. According to presented results of reliability analysis, it is found that distribution types of variables have little influence on risk analysis. However, the *COVs* values of uncertainties have different influences on reliability results when the slopes are in different situations. It is also shown that the magnitudes of two constants (*D*, k_h) could have significant effect on the P_f estimation.

In order to provide guidance for slope designs with the help of reliability analysis, the relationship between probability of failure and mean safety factor is investigated. It is found that the relation between P_f and μ_F is independent of the magnitudes of input parameters but relative to the variability of variables. Therefore, the *COVs* values should be determined by sufficient experimental and field measured data, so as to obtain actual curves in Fig. 13 for slope designs. If no further sample and data information is available, designers can adopt the curve based on the *COVs* values.

Reference

Al-Homoud, A.S. and Tanash, N. (2004), "Modeling uncertainty in stability analysis for design of embankment dams on difficult foundations", *Eng. Geol.*, **71**(3), 323-342.

Cai, M., Kaiser, P.K., Tasaka, Y. and Minami, M. (2007), "Determination of residual strength parameters of jointed rock masses using the GSI system", *Int. J. Rock Mech. Min. Sci.*, **44**(2), 247-265.

Cassidy, M.J., Uzielli, M. and Lacasse, S. (2008), "Probability risk assessment of landslides: A case study at Finneidfjord", *Can.*

Geotech. J., **45**(9), 1250-1267.
Griffiths, D.V. and Marquez, R.M. (2007), "Three-dimensional slope stability analysis by elasto-plastic finite elements", *Geotechnique*, **57**(6), 537-546.
Hoek, E. (1998), "Reliability of Hoek-Brown estimates of rock mass properties and their impact on design", *Int. J. Rock Mech. Min. Sci.*, **35**(1), 63-68.
Hoek, E. and Brown, E.T. (1980), "Empirical strength criterion for rock masses", *J. Geotech. Eng. Div.*, **106**(9), 1013-1035.
Hoek, E., Carranza-Torres, C. and Corkum, B. (2002), "Hoek-Brown failure criterion-2002 edition", *Proceedings of NARMS-TAC*, **1**, 267-273.
Huang, X.L., Zhou, Z.G. and Yang, X.L. (2018), "Roof failure of shallow tunnel based on simplified stochastic medium theory", *Geomech. Eng.*, **14**(6), 571-580.
Hungr, O. (1987), "An extension of Bishop's simplified method of slope stability analysis to three dimensions", *Geotechnique*, **37**(1), 113-117.
Li, A.J., Cassidy, M.J., Wang, Y., Merifield, R.S. and Lyamin, A.V. (2012), "Parametric Monte Carlo studies of rock slopes based on the Hoek-Brown failure criterion", *Comput. Geotech.*, **45**, 11-18.
Li, K.S. and Lumb, P. (1987), "Probabilistic design of slopes", *Can. Geotech. J.*, **24**(4), 520-535.
Li, T.Z. and Yang, X.L. (2018a), "Risk assessment model for water and mud inrush in deep and long tunnels based on normal grey cloud clustering method", *KSCE J. Civil Eng.*, **22**(5), 1991-2001.
Li, Z.W. and Yang, X.L. (2018b), "Stability of 3D slope under steady unsaturated flow condition", *Eng. Geol.*, **242**, 150-159.
Low, B.K. (2007), "Reliability analysis of rock slopes involving correlated nonnormals", *Int. J. Rock Mech. Min. Sci.*, **44**(6), 922-935.
Luo, W.H. and Li, W.T. (2016), "Reliability analysis of supporting pressure in tunnels based on three-dimensional failure mechanism", *J. Central South Univ.*, **23**(5), 1243-1252.
Michalowski, R.L. (1989), "Three-dimensional analysis of locally loaded slopes", *Geotechnique*, **39**(1), 27-38.
Michalowski, R.L. and Drescher, A. (2009), "Three-dimensional stability of slopes and excavations", *Geotechnique*, **59**(10), 839-850.
Shinoda, M. (2007), "Quasi-Monte Carlo simulation with low-discrepancy sequence for reinforced soil slopes", *J. Geotech. Geoenviron. Eng.*, **133**(4), 393-404.
Xu, J.S., Li, Y.X. and Yang, X.L. (2018), "Stability charts and reinforcement with piles in 3D nonhomogeneous and anisotropic soil slope", *Geomech. Eng.*, **14**(1), 71-81.
Xu, J.S. and Yang, X.L. (2018a), "Effects of seismic force and pore water pressure on three dimensional slope stability in nonhomogeneous and anisotropic soil", *KSCE J. Civil Eng.*, **22**(5), 1720-1729.
Xu, J.S. and Yang, X.L. (2018b), "Three-dimensional stability analysis of slope in unsaturated soils considering strength nonlinearity under water drawdown", *Eng. Geol.*, **237**, 102-115.
Yang, X.L. and Li, Z.W. (2018a), "Kinematical analysis of 3D passive earth pressure with nonlinear yield criterion", *Int. J. Numer. Anal. Meth. Geomech.*, **42**(7), 916-930.
Yang, X.L. and Li, Z.W. (2018b), "Upper bound analysis of 3D static and seismic active earth pressure", *Soil Dyn. Earthq. Eng.*, **108**, 18-28.
Yang, X.L. and Wang, H.Y. (2018), "Catastrophe analysis of active-passive mechanisms for shallow tunnels with settlement", *Geomech. Eng.*, **15**(1), 621-630.
Yang, X.L. and Zhang, S. (2018a), "Risk assessment model of tunnel water inrush based on improved attribute mathematical theory", *J. Central South Univ.*, **25**(2), 379-391.
Yang, X.L. and Zhang, R. (2018b), "Limit analysis of stability of twin shallow tunnels considering surface settlement", *KSCE J. Civil Eng.*, **22**(5), 1967-1977.
Zhang, D.B. and Sun, Z.B. (2013), "Reliability analysis of retaining walls with multiple failure modes", *J. Central South Univ.*, **20**(10), 2879-2288.
Zhang, X.J. and Chen, W.F. (1987), "Stability analysis of slopes with general nonlinear failure criterion", *Int. J. Numer. Anal. Meth. Geomech.*, **11**(1), 33-50.

CC